Phase transition from pseudomorphic $FeSi_2$ to β-$FeSi_2$/Si(111) studied by *in situ* scanning tunneling microscopy

H. Sirringhaus, N. Onda, E. Müller-Gubler, P. Müller, R. Stalder, and H. von Känel
Laboratorium für Festkörperphysik, Eidgenössische Technische Hochschule Zürich, CH-8093 Zürich, Switzerland
(Received 14 July 1992)

We have used the scanning tunneling microscope to study the Jahn-Teller-like structural transition from pseudomorphic $FeSi_2$ on Si(111) to the stable bulk phase β-$FeSi_2$. Thin films of the pseudomorphic phase have been grown by molecular-beam epitaxy at room temperature. The crystal structure has been determined to be a CsCl-derived defect phase with a statistical occupation of the metal sites. In scanning tunneling spectroscopy we have found direct evidence for the atomic disorder on the metal sublattice. The fluorite structure was only observed after prolonged annealing at temperatures near the transition to β-$FeSi_2$. Upon annealing the crystalline order deteriorates when approaching the transition, which manifests itself in the appearance of a smooth surface corrugation on a 100-Å scale in scanning-tunneling-microscope topographs. This can be explained by a precursor phase in which the cubic silicide is locally distorted towards orthorhombic β-$FeSi_2$. The actual transition is very sensitive to kinetic factors, i.e., the stoichiometry of the initial deposit. Apart from the (101) orientation of β-$FeSi_2$ occurring also in films grown by solid-phase epitaxy both a (001) and a (100) orientation have been observed. The corresponding films exhibit a high degree of structural perfection with grains several μm in size which might become relevant to electro-optical applications. We discuss the surface reconstructions observed on the various types of β-$FeSi_2$ grains.

I. INTRODUCTION

In its stable bulk form at room temperature $FeSi_2$ is a semiconductor with a direct band gap of 0.87 eV. Since it can be grown epitaxially on Si(111) and (100) it has become a promising candidate for optoelectronic applications in Si technology.[1,2] This so-called β-$FeSi_2$ phase has an orthorhombic crystal structure belonging to the *Cmca* space group; it can be understood as a Jahn-Teller distortion of a cubic $FeSi_2$ phase with the fluorite structure.[3] The geometric misfit to Si is relatively large; the volume of the unit cell is smaller by -6.1% than that of the four corresponding fluorite cells with the Si lattice constant. Systems with large misfit can sometimes adopt a different crystal structure which does not occur in the bulk phase diagram but which can be synthesized in thin-film form. This may happen when the new phase is well lattice matched to the substrate. The phenomenon is called pseudomorphism and was observed for a variety of systems, such as bcc Co on GaAs.[4] Recently, the synthesis of a cubic, metallic $FeSi_2$ phase on Si(111) has been achieved by solid-phase epitaxy (SPE),[5] liquid-phase epitaxy (LPE),[6] and molecular-beam epitaxy (MBE).[7] A band-structure calculation by Christensen on a hypothetical $FeSi_2$ phase with the CaF_2 structure[8] predicted a lattice constant equal to that of Si to within 1%. From a practical point of view, research in this field has been mainly motivated by Christensen's finding that fluorite $FeSi_2$ might be a Stoner ferromagnet.

In this work cubic $FeSi_2$ films were grown by MBE at room temperature (RT) and the phase transition from the pseudomorphic to the stable bulk phase β-$FeSi_2$ was studied by *in situ* scanning tunneling microscopy (STM) and transmission electron microscopy (TEM). In several respects the $FeSi_2$ system is ideal for a study of this kind of transformation since cubic $FeSi_2$ films grown by MBE exhibit a high degree of structural perfection, the growth mode being two dimensional up to film thicknesses of at least 60 Å. Furthermore, the phase transition can be induced by annealing which allows one to carefully trace the detailed path which the system follows. We first determined the crystal structure of the as-grown samples and found it to have the CsCl symmetry (see Sec. III A). Upon annealing a gradual decrease in the long-range periodic order was observed, i.e., the structural properties were found to vary laterally on a 100-Å scale (see Sec. III B). This state preceded the actual transformation. Our explanation in terms of a local distortion of the cubic towards the orthorhombic phase sheds light on the contradictory results reported on the crystal structure of the cubic phase.[5–7] The phenomenon might also occur in other pseudomorphic systems. The way in which the actual phase transition to β-$FeSi_2$ proceeds was found to be very sensitive to kinetic factors, i.e., to slight variations in the stoichiometry of the initial deposit (see Sec. III C). Apart from the epitaxial orientations observed in SPE-grown films two additional ones with comparatively low lattice mismatch have been observed. The corresponding β-$FeSi_2$ films are almost two dimensional with a grain size of several μm; this might become relevant for practical applications, since SPE-grown films usually suffer from a rather poor morphology.[9] We present a detailed STM study of the surface reconstructions on the different β-$FeSi_2$ grains.

II. EXPERIMENT

$FeSi_2$ films with thicknesses between 5 and 300 Å were grown in a commercial 3-in. MBE machine on Si(111)

substrates (*n*-doped, 1–2000 Ω cm). The substrate preparation technique, described in detail in Ref. 10, resulted in clean, 7×7 reconstructed surfaces with parallel monolayer (ML) steps due to the unintentional wafer misorientation of 0.1°–0.3°. In a first step an ultrathin crystalline template was grown as a seed by depositing 2 Å of Fe followed by the deposition of 7 Å $FeSi_2$ by stoichiometric coevaporation onto the substrate held near RT. The materials were electron-gun evaporated at a deposition rate of 0.3 Å/s for Fe and 1 Å/s for Si. Rates were monitored by quartz balances and stabilized to within 5–10%. The templates were annealed at 450–500 °C. Temperatures were measured by a thermocouple calibrated by an optical pyrometer for $T > 400$ °C. In a second step the desired film thickness was reached by stoichiometric coevaporation at RT. The films were characterized *in situ* by reflection high-energy electron diffraction (RHEED), ultraviolet and x-ray-photoelectron spectroscopy (UPS/XPS), and STM. The STM setup has been described elsewhere.[11] PtIr tips were used which were routinely cleaned by Ar sputtering. The TEM measurements were performed in a JEM JEOL 200CX (high tension 200 kV). Samples for the plan-view investigations were prepared by chemical etching, cross sections by cleaving.

III. RESULTS AND DISCUSSION

A. Crystal structure at RT

Templates formed at RT exhibit a 1×1 RHEED pattern with well-developed Kikuchi bands of cubic symmetry revealing type-B orientation of the silicide, i.e., the silicide is rotated by 180° around the Si(111) direction. During the second codeposition step the sharp Kikuchi band pattern remains, demonstrating epitaxial growth at RT.

Figure 1 shows a cross-sectional TEM diffraction pattern obtained from an as-grown $FeSi_2$ layer with a thickness of 80 Å. If the silicide spots are indexed with respect to a simple cubic unit cell with the Si lattice parameter all (*hkl*) reflexes with odd indices are absent. The silicide spots are separated from the Si ones due to the type-B orientation. This was confirmed by x-ray diffraction (XRD) and a detailed analysis of Kikuchi band panoramas. From these results we can exclude the CaF_2 structure. The diffraction pattern is consistent with a CsCl symmetry of the silicide, the lattice constant being half as large as that of Si. Recently, we have reported on the successful synthesis of a pseudomorphic, metallic FeSi phase on Si(111) with the CsCl structure.[12] It is stabilized with respect to the stable bulk form, ϵ-FeSi, by a favorable interface structure. The geometrical lattice mismatch is $\eta \simeq 2\%$ as determined by XRD. By measuring the thickness evolution from TEM cross sections and by monitoring the core-level intensities in XPS we showed that the stoichiometry in ultrathin FeSi films evolves towards 1:2 upon annealing to 500 °C. This transformation occurs without any change in symmetry. The surface structure observed in STM topographs was the same as for annealed samples grown intentionally with 1:2 stoichiometry (see Sec. III B). This suggests that the low-temperature form of $FeSi_2$ is a CsCl-derived defect phase, where all metal sites are equivalent due to statistical occupation. Such a defect $Fe_{1-x}Si$ phase can be grown epitaxially at RT in the whole stoichiometry range from $x = 0$ up to at least $x = 0.6$. On the Fe-rich side one can successively replace Si by Fe up to type-B oriented bcc Fe.[13]

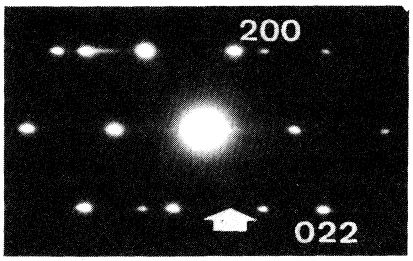

FIG. 1. Cross-sectional TEM diffraction pattern of an as-grown $FeSi_2$ film with the CsCl symmetry taken along the $[01\bar{1}]$ direction. Only the silicide spots are indexed according to a cubic cell with the Si lattice parameter.

STM was of limited use for the as-grown samples. On a mesoscopic scale two-dimensional layer-by-layer growth was observed with contrast due to the substrate surface steps remaining visible up to film thicknesses of at least 60 Å. On an atomic scale the surface exhibited a 1–2-Å roughness due to the low surface mobility at RT which does not admit a well-ordered surface structure.

B. Evolution of the crystal structure upon annealing

Figure 2(a) illustrates the typical surface morphology of $FeSi_2$ films after annealing at 500 °C. Within the 4-μm lateral range of our scanner the films are smooth. Pinhole formation can be avoided by preparing the surface slightly Si-rich (in analogy to the enhanced thermal stability of Si-rich surfaces in the $CoSi_2$ system[10]). Two kinds of misorientation-induced steps can be distinguished: true surface steps with an abrupt profile and rather smooth, buried steps. The latter are 1.6 Å high but do not lead to a disruption of the atomic surface structure. They are rather straight in contrast to the faceted surface steps. Corresponding TEM plan-view measurements resolved an array of parallel dislocations with an average distance determined by the wafer misorientation. We conclude that the buried steps are due to dislocations formed at the silicon-silicide interfacial steps. The topographic contrast observed on the surface implies that the Burgers vector has a component perpendicular to the interface plane. The occurrence of dislocations associated with interfacial steps is a consequence of the type-B orientation of the silicide. The height of the surface steps as well as that of ML islands and holes on the terraces is also 1.6 Å. Since we observed no differences in the atomic structure of the adjacent planes, this is consistent with the CsCl symmetry of the silicide for which the distance between equivalent (111) planes is half the one in the CaF_2 structure.

The terraces in Fig. 2(a) are not homogeneous but ex-

hibit a smooth contrast on a 100-Å scale, on which we will focus now. During annealing above 400–450 °C the Kikuchi bands observed by RHEED become more and more diffuse for films thicker than ~10–15 Å. By 500 °C most bands have almost completely vanished. In Rutherford backscattering spectrometry (RBS) the silicide channeling minima are completely lost. This drastic deterioration in the crystalline order of the bulk silicide is accompanied by the appearance of the fine-scale, speckle contrast in STM topographs which is more clearly resolved in Fig. 2(b). Obviously, this 21-Å-thick film has become laterally inhomogeneous. The surface exhibits a smooth corrugation with an amplitude of ~0.8–1 Å. Its wavelength, i.e., the characteristic distance between adjacent hills or valleys, was measured to be of the order of ~80 Å.

The faint atomic-scale corrugation, which is barely resolved in Fig. 2(b), is due to a 2×2 surface reconstruction. The corresponding additional RHEED reflexes appear around 300 °C. By 350 °C they have become as intense as the low-temperature 1×1 spots. Upon further annealing they remain up to the transition to β-$FeSi_2$. The high-resolution STM topographs in Fig. 3 stem from a 16-Å $FeSi_2$ film annealed at 500 °C. The empty-state image [Fig. 3(a)] displays a perfectly ordered, hexagonal 2×2 reconstruction with a corrugation amplitude of 0.4 Å. The system exhibits the peculiar phenomenon of a well-ordered surface in spite of deteriorating crystalline quality and lateral strain variations in the bulk. The 2×2 has already been described in a STM study of SPE-grown $FeSi_2$.[14] It has been attributed to a termination of the silicide by Si adatoms with a configuration similar to the one of adatoms on the Si(111)-7×7.

The large-scale waviness does not seem to influence or disrupt the atomic reconstruction. Two kinds of domain boundaries are visible between the four equivalent domains of the 2×2 in Fig. 3. Type-I boundaries make an angle of 60° with the relative displacement vector $\mathbf{\Delta}=(a/2)\langle 1\bar{1}0\rangle$ ($\Delta=3.8$ Å) of the two adjacent domains. They appear as dark ditches and are also resolved in Fig. 2(b). Type-II boundaries run parallel to $\mathbf{\Delta}$. The average domain size was found to scale with the wavelength of the surface corrugation. We attribute this fact to the surface strain caused by the corrugation, which leads to an increase of the mean distance between nearest-neighbor atoms with respect to the uncorrugated surface. It has to be pointed out that no direct correspondence between the location of the domain boundaries and crests and valleys could be established.

While in the empty-state image, Fig. 3(a), all atomic protrusions appear to be equivalent, the corresponding

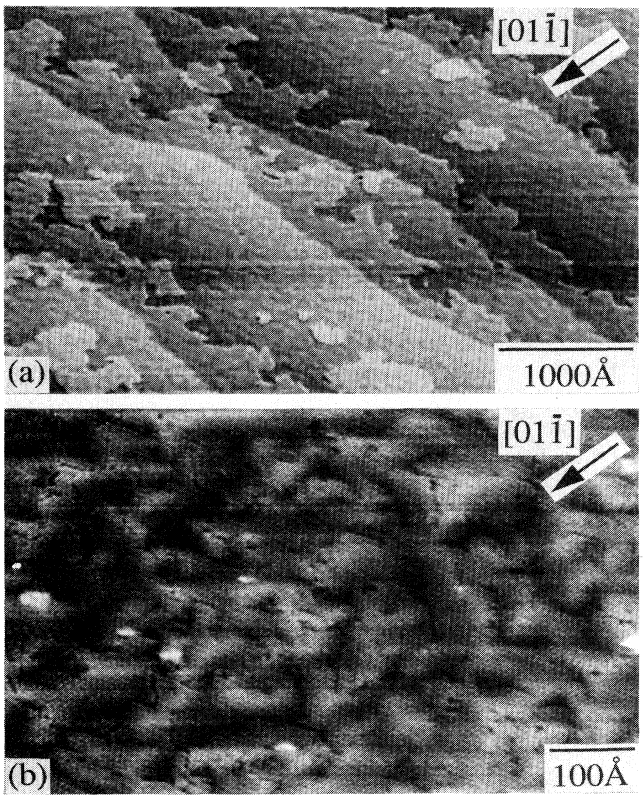

FIG. 2. STM topographs obtained on pseudomorphic $FeSi_2$ displaying (a) the mesoscopic surface morphology (sample bias voltage $V_t=1$ V, tunneling current $I_t=1$ nA, film thickness $d=21$ Å, annealing temperature $T_a=500$ °C) and (b) the surface corrugation ($V_t=1.5$ V, $I_t=2$ nA, $d=21$ Å, $T_a=500$ °C).

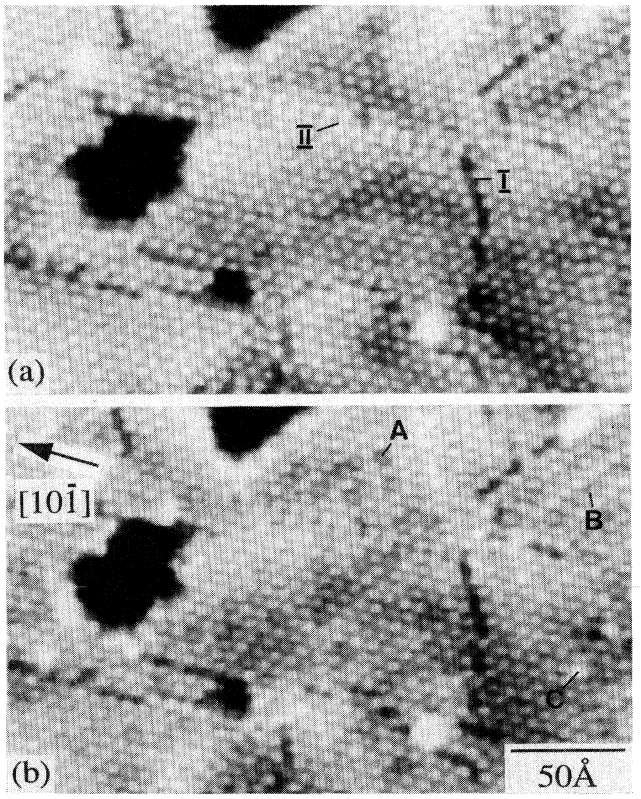

FIG. 3. Atomic resolution STM topographs of the 2×2 surface reconstruction ($d=16$ Å, $T_a=500$ °C): (a) empty-state image ($V_t=2$ V, $I_t=0.5$ nA), (b) filled-state image ($V_t=-2$ V, $I_t=0.5$ nA). I and II denote the two different types of 2×2 domain boundaries. Sites with significant voltage dependencies are labeled by letters.

filled-state image, Fig. 3(b), reveals considerable inhomogeneities: Many of the adatoms seem to be slightly depressed. They can either be isolated (A) or form rows (B). In addition, a few adatoms appear much brighter (C). This is possibly due to local adsorption of residual gas atoms[15] (see below).

These atomic-scale contrast variations are even more drastic on films with thicknesses below 10 Å. Such layers could be annealed up to 500 °C without any deterioration in Kikuchi band intensity and the surface corrugation described above was not detected. Therefore we believe that the atomic-scale contrast is not directly related to the smooth surface corrugation. Current-imaging tunneling spectroscopy[16] (CITS) was performed to investigate the origin of the inequivalence among the 2×2 adatom sites. Figures 4(a) and 4(b) show empty- and filled-state

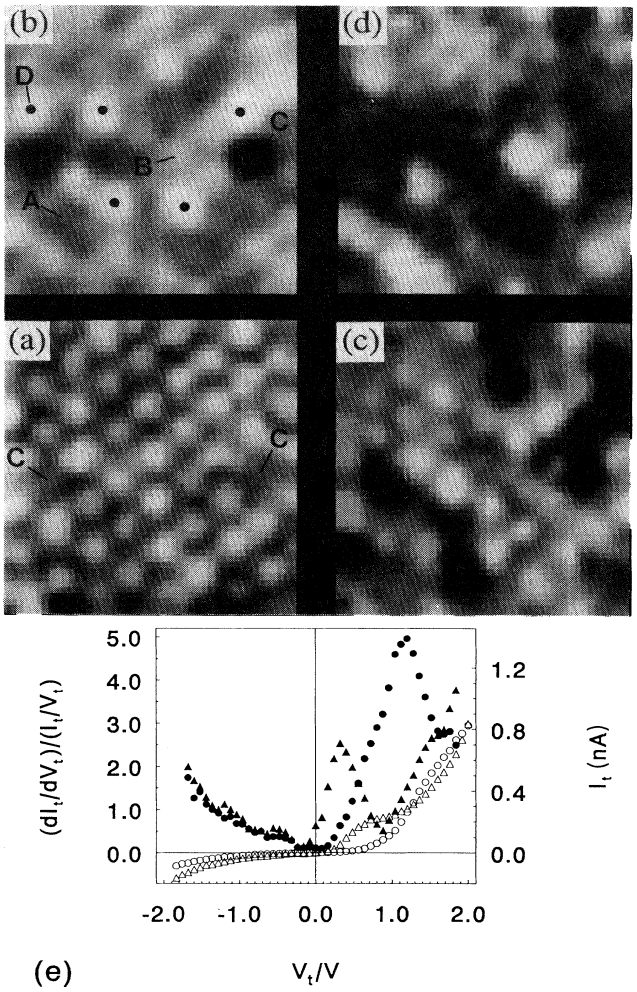

FIG. 4. Constant-current topographs (CCT) and current images (CI) of the 2×2 on ultrathin films ($d=7$ Å, $T_a=500$ °C): (a) empty-state CCT ($V_t=2$ V, $I_t=1$ nA), (b) filled-state CCT ($V_t=-2$ V, $I_t=1$ nA), (c) CI at $V_t=1.35$ V, (d) CI at $V_t=0.3$ V measured with a stabilization voltage and current of 2 V and 1 nA, respectively (in the CI, areas of high current appear bright), (e) current-voltage (open symbols) and normalized conductivity (filled symbols) curves belonging to the depressed (A, circles) and bright (B, triangles) sites of the filled-state CCT in (b).

constant-current topographs (CCT) of the 2×2 reconstruction obtained on a 7-Å $FeSi_2$ film annealed at 500 °C. In the empty-state image again all sites are equivalent, except for two point defects (C) with missing adatoms. In the filled-state image the individual atoms are less clearly resolved. Ordinary CCT with a higher density of sampling points revealed that the darker sites (A) do indeed correspond to depressed adatoms similar to the ones in Fig. 3(b). The corresponding current images (CI) belonging to a stabilization voltage of +2 V are shown in Figs. 4(c) and 4(d) for tunneling voltages of 1.35 and 0.3 V, respectively. Obviously, the surface electronic structure varies locally without any relationship to the 2×2 periodicity.

In order to further clarify the origin for this high degree of disorder we have compared normalized conductivity spectra $(dI_t/dV_t)/(I_t/V_t)_{\text{ave}}$ in order to partly eliminate the influence of the energy dependence of the tunneling transmission factor. The derivatives were calculated numerically with the help of quadratic least-squares fits. The conductance I_t/V_t was averaged by convolution with a smoothing function. In reciprocal space a Fermi function was used, which was found to be more appropriate for the rather low density of 50 sampling points per spectrum than the one-pole, low-pass filter proposed by Stroscio and Feenstra.[17]

In general, all $I(V)$ curves, which were taken at constant separation, show a strong overall asymmetry between positive and negative voltages, which has often been reported for scanning tunneling spectra.[18] On the depressed sites in the filled-state CCT (A) spectra like the one shown in Fig. 4(e) (open and filled circles) were obtained. They are characterized by a prominent peak at ~1.2 V with a second one on the low-energy shoulder varying in position between 0.6 and 0.8 V. The spectra measured on the bright sites in the filled-state CCT [position B, triangles in Fig. 4(e)] are qualitatively different: They always exhibit a distinct peak at ~0.3 V, which is kind of a fingerprint since it does not occur on the depressed sites. Around 1.5 V another weaker feature appears. The topographic contrast variations in the filled-state CCT are not directly related to density-of-states (DOS) features since on all sites the conductivity appears rather featureless in the negative voltage range. Nevertheless, the occurrence of the DOS peak at 0.3 V on B is accompanied by a stronger exponential current increase with V_t becoming more negative than on A [see Fig. 4(e), open symbols]. This implies that in a filled-state CCT the tip has to come closer to the surface on A than on B to reach the regulating current, which leads to the observed topographic contrast differences. These variations in the overall current increase must be less pronounced for positive voltages since the empty-state CCT is rather homogeneous. It is of course difficult to prove this directly because by using a negative stabilization voltage one would have to compare spectra taken with different tip-sample distances. In our discussion we have disregarded spectra measured on sites C and D. These differ from the remaining ones in that they are featureless over the entire voltage range. This might be accounted for by missing adatoms (C) and adsorption sites (D).[15] On sites D which

appear similar to the isolated bright adatoms in Fig. 3(b) the current at negative V_t increases much more strongly than on the other sites.

As a conclusion we state that the surface DOS exhibits variations on an atomic scale. This is in accordance with our model of the crystal structure of the pseudomorphic phase. For a defect CsCl phase with statistical occupation of metal sites one can expect vacancies in the first metal layer below the surface which will certainly lead to variations in the surface electronic structure.

We will now come back to the surface corrugation and describe how it depends on film thickness and annealing temperature. The tendency towards crystal structure deterioration was found to be more pronounced for thicker films. These already exhibit rather diffuse Kikuchi band patterns at relatively low annealing temperatures and the amplitude of the surface corrugation is enlarged: For a 40-Å film annealed at 450 °C it is of the order of 1.5–2 Å. This has to be compared with the value of 0.8–1 Å for the 21-Å film of Fig. 2(b) or 0.5 Å for the 16-Å film of Fig. 3. This observation confirms that the effect is related to inhomogeneities in the bulk silicide.

Some samples were annealed in several steps in order to investigate how the surface morphology evolves as a function of the annealing temperature. First, an increase of the corrugation wavelength was observed: after annealing at 550 °C it has become as large as 150–200 Å for the 17-Å film shown in Fig. 5(a), while its amplitude is still of the order of 1 Å. The crests and valleys tend to be oriented along the Si$\langle 2\bar{1}\,\bar{1}\rangle$ directions. They appear rather localized, leaving planar, essentially homogeneous regions between them. Figure 5(b) displays the same sample after further annealing at 600 °C, which was already close to the transition to β-$FeSi_2$, i.e., $\sim 10\%$ of the surface was covered with β-$FeSi_2$ grains. A qualitative change in the defect structure of the film was observed: the surface corrugation has almost disappeared; instead, screwlike defects occur, like the one indicated by the arrow in the middle left of the figure. In addition, buried steps like the ones in Fig. 2(a) appear on the terraces (see lower left). The density of surface steps has increased drastically. Most of them are still 1.6 Å high, whereas some have double height. It is important to note that the quality of the cubic Kikuchi band pattern (which continuously deteriorated during the annealing, as described above) does not improve, even after prolonged annealing. (The formation of the little pinholes can be avoided by depositing several Å of Si onto the silicide before annealing.) On the atomic scale filled- and empty-state CCT's display a perfectly homogeneous 2×2 reconstruction, which suggests that at least at the surface ordering on the metal sublattice takes place (cf. D). The 2×2 domain boundaries and the surface steps are often decorated by linear chains of adatoms oriented along the Si$\langle 01\bar{1}\rangle$ direction [Fig. 5(b)]. They probably consist of outdiffused excess Si. In general, the microscopic surface structure at such high annealing temperatures is similar to the one reported for the SPE-grown samples.[14] In this respect it has to be pointed out that the long-ranged surface corrugation has not been reported in Ref. 14. This might be partly due to the high temperatures at which crystallization occurs in SPE and the limitation to relatively thin films with $d<20$ Å (Ref. 5). In addition, SPE-grown films consist of individual crystallites of only some 100 Å in size.

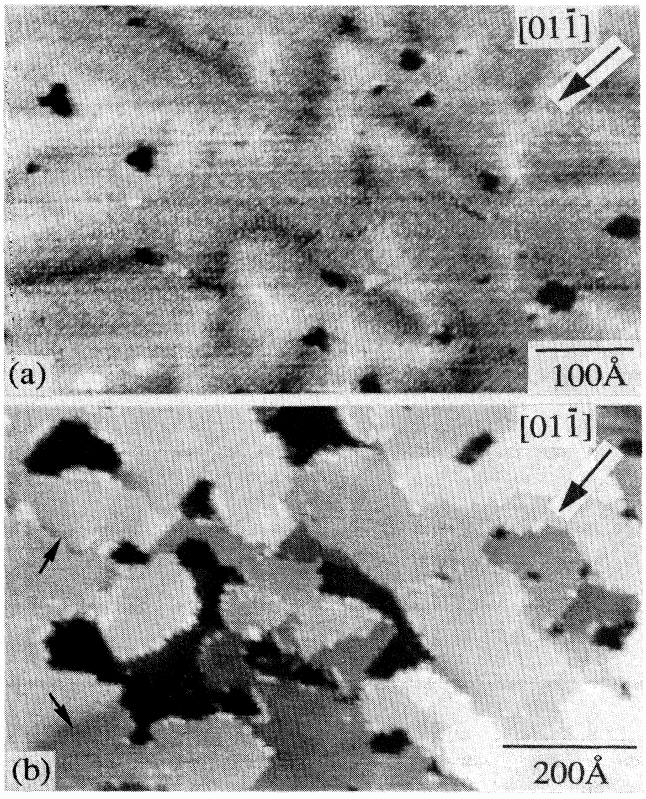

FIG. 5. STM topographs illustrating the evolution of the surface corrugation at higher annealing temperatures ($d=17$ Å): (a) after 550 °C ($V_t=1.6$ V, $I_t=1$ nA), (b) after 600 °C ($V_t=1.8$ V, $I_t=0.5$ nA).

C. Transition to β-$FeSi_2$

If one further increases the annealing temperature the transition to β-$FeSi_2$ occurs. In a certain temperature range the two phases coexist [Fig. 6(a)]. Three epitaxial orientations with drastically different nucleation behavior were distinguished. The path which the system follows was found to be extremely sensitive to slight variations in the composition of the initial deposit.

1. β-$FeSi_2$(101) ‖Si(111)

The same epitaxial orientation as that reported for SPE-grown samples (β-$FeSi_2(101)$‖Si(111) with β-$FeSi_2[010]$‖Si$\langle 0\bar{1}1\rangle$) dominates on stoichiometrically grown films (i.e., with an Fe:Si coevaporation ratio of 1:2). It results in a relatively large mismatch of -5.3% along Si$\langle 2\bar{1}\,\bar{1}\rangle$ and 1.4% along Si$\langle 0\bar{1}1\rangle$. The phase transition proceeds by nucleation of isolated β-$FeSi_2$ grains with relatively small size (typically 1000 Å in diameter) within the cubic matrix. Figure 6(a) shows an example for a 31-Å-thick film annealed at 500 °C. On the terraces of the remaining cubic silicide the faint speckle contrast

due to the surface corrugation is still resolved. The β-$FeSi_2$ grains occur in all three equivalent orientations expected from the threefold symmetry of the Si[111] direction. This is apparent from the slight tilt towards the Si$\langle 11\bar{2}\rangle$ direction of the β-$FeSi_2$ surface planes with respect to the (111) planes of the cubic precursor phase. This leads to an increased density of surface steps of predominantly ~3-Å height running along Si$\langle 01\bar{1}\rangle$. At higher annealing temperatures the density of these grains increases, leading eventually to multidomain β-$FeSi_2$ films with rather poor morphology.

On an atomic scale such grains exhibit partly disordered regions where no periodic order could be resolved. In other areas a rather interesting surface reconstruction was observed, which is shown in Fig. 6(b). It consists of an alternating array of two different structures with straight domain boundaries running along the characteristic Si$\langle 01\bar{1}\rangle$ surface steps on the grain. Domains of type A are predominant while type-B domains are sometimes only some 10 Å wide. For a discussion of the epitaxial orientation we choose a primitive surface unit cell on each domain with side lengths of $u=14.8$ Å, $v=9.8$ Å, and an angle of 80° between the two basis vectors. The reconstruction is easy to resolve due to a large corrugation amplitude, e.g., typically 0.8–1 Å along the v side. All corrugation maxima have an asymmetric dimerlike structure perpendicular to the v side which has been reproducibly observed on several samples. One possibility to transform the two domains into each other is to perform a mirror reflection in a plane perpendicular to the domain boundary (indicated by a dashed line) with a subsequent in-plane translation $\mathbf{t}$ by ~6 Å. This is in accordance with the β-$FeSi_2$ space-group symmetry if one assumes that the exposed surface plane is indeed a (101) plane (in spite of its tilt): Perpendicular to the b axis there is a glide plane running through the center of the unit cell (if chosen as in Fig. 7). The corresponding translation vector $\mathbf{t}=(\mathbf{a}-\mathbf{c})/2$ lies in the (101) plane. This symmetry element is a combination of a twofold rotation around the a axis and the a glide plane perpendicular to the c axis. Hence the two domains can be understood as equivalent reconstructions related by a symmetry operation of the unreconstructed surface.

The above-mentioned tilt of the β-$FeSi_2$ surface planes is difficult to explain. It is not uniform over the whole grain. The maximum inclination was measured to be ~2° towards Si$\langle 11\bar{2}\rangle$. But there are also areas where the

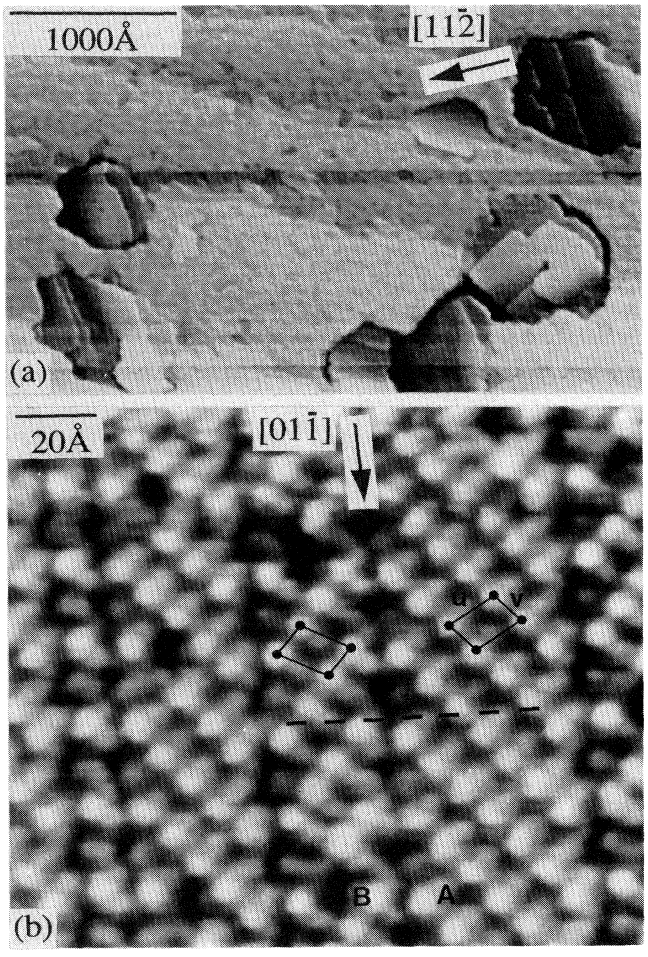

FIG. 6. STM topographs of (101)-oriented β-$FeSi_2$ grains: (a) nucleation of β-$FeSi_2$ grains within the cubic matrix ($d=31$ Å, $T_a=500$ °C, $V_t=1.5$ V, $I_t=1$ nA), (b) empty-state CCT of the surface reconstruction ($d=53$ Å, $T_a=630$ °C, $V_t=2$ V, $I_t=4$ nA) (in all STM images directions are indexed with respect to the Si substrate). The unit cells (solid lines) on domains A and B can be transformed into each other by a glide plane operation. The dashed line indicates the line of intersection of the mirror plane with the surface.

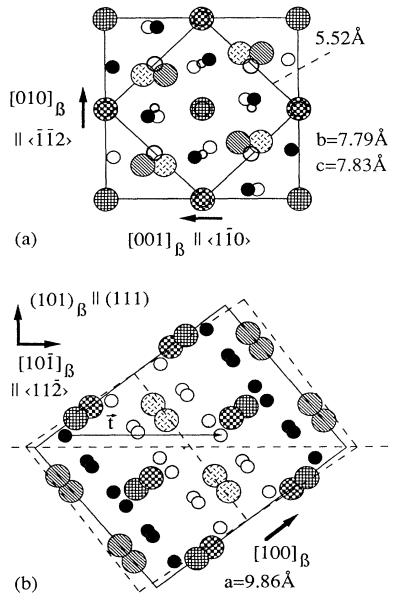

FIG. 7. Schematic drawing of the β-$FeSi_2$ unit cell: (a) (100) projection, the corresponding atomic positions in the fluorite structure are indicated by solid lines, (b) (010) projection, the horizontal is thought to represent the Si(111) interface. The two corresponding CaF_2 unit cells are shown in dashed lines (all β-$FeSi_2$ directions are given with respect to the Si substrate according to the epitaxial orientations described in the text).

surface plane is not inclined. Between tilted and nontilted regions the surface is smoothly bent. This suggests that the atomic structure at the β-$FeSi_2$/Si interface varies laterally, which requires rather abnormal elastic properties of the orthorhombic phase. Another interesting observation is that stoichiometric films thinner than $\sim$30 Å become discontinuous above 600 °C, exposing large areas of the bare Si substrate. In contrast, the other two epitaxial orientations to be discussed in the following are completely wetting up to at least 650 °C.

2. β-$FeSi_2$ (001) ‖Si (111)

If the initial deposit is slightly Fe rich (Fe:Si$\approx$1:1.5) and if the films are heated up cautiously with prolonged annealing at temperatures around 500 °C, films thinner than $\sim$35 Å exhibit a quasicontinuous phase transition to β-$FeSi_2$ which preserves the smooth surface morphology of the cubic precursor phase. The first β-$FeSi_2$ RHEED reflexes appear already at comparatively low temperatures around 480–500 °C. The RHEED pattern is of sixfold symmetry indicating a twofold-symmetric surface reconstruction with grains occurring in all three equivalent orientations. By TEM the typical grain size diameter was determined to be of the order of 6 μm. The surface morphology on each grain is characterized by an array of parallel, $\sim$4-Å-high surface steps with a distance corresponding to the wafer misorientation [see Fig. 8(b)]. UPS and scanning tunneling spectroscopy have clearly proven the semiconducting nature of this phase. By TEM plan-view diffraction [see Fig. 8(a)] we determined the epitaxial orientation of such grains to be β-$FeSi_2$(001)‖Si(111) with β-$FeSi_2$[100]‖Si$\langle 11\bar{2}\rangle$. This results in a relatively small geometric misfit of -1.2% along Si$\langle 11\bar{2}\rangle$ and 1.4% along Si$\langle 01\bar{1}\rangle$, which might compensate for an unfavorable atomic arrangement at the Si-silicide interface. The common unit mesh is also reasonably small ($2a\times b = 19.7$ Å$\times 7.8$ Å). On metallic $CoSi_2$ on Si we have recently observed that interfacial misfit dislocations induce a topographic contrast on the surface by which the strain relaxation can be investigated with STM.[19] The semiconducting β-$FeSi_2$(001) grains exhibit the same kind of contrast. We detected two nearly orthogonal sets of parallel dislocations with an average distance around 120 and 200 Å, respectively. From this we conclude that the β-$FeSi_2$ grains are at least partly relaxed, which has been confirmed by TEM Moiré pattern analysis. It should be mentioned that the (001) orientation, which does not occur in SPE-grown films, has also been reported for buried β-$FeSi_2$ films prepared by ion-beam synthesis.[20]

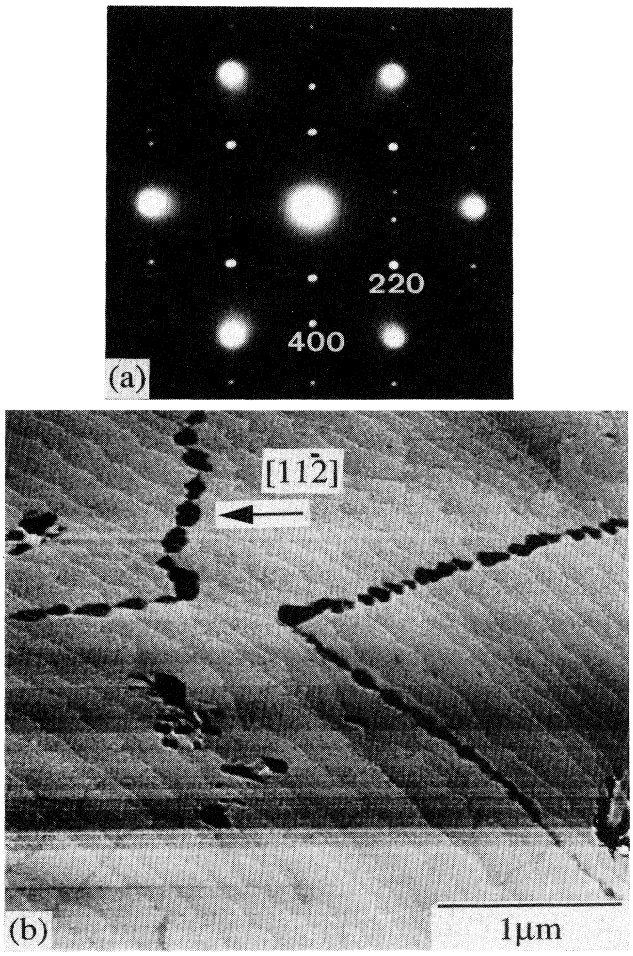

FIG. 8. (a) Selected-area plan-view TEM diffraction pattern of (001)-oriented β-$FeSi_2$ ($d=26$ Å, $T_a=480$ °C) taken along Si[111]. The bright spots with sixfold symmetry are the Si$\{02\bar{2}\}$ spots, (b) large area STM topograph ($V_t=2$ V, $I_t=1$ nA) obtained on a 53-Å-thick β-$FeSi_2$ film grown by using a (001)-oriented β-$FeSi_2$ film with 31-Å thickness as a template ($T_a=550$ °C).

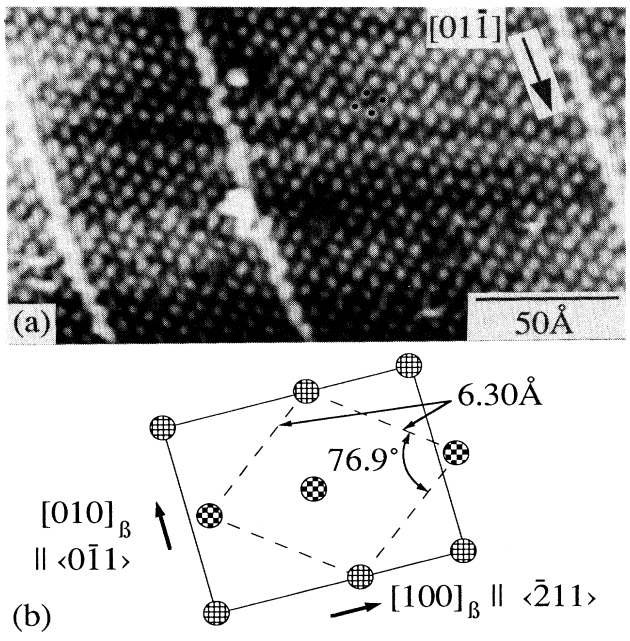

FIG. 9. (a) Empty-state CCT displaying the surface reconstruction on (001)-oriented β-$FeSi_2$ ($V_t=0.2$ V, $I_t=0.2$ nA, $d=26$ Å, $T_a=600$ °C). A surface unit cell is indicated by black dots, (b) schematic model for the reconstruction in (a) based on the Fe(001) planes shown checkered in Fig. 7(b). The unit cell observed in STM is indicated by dashed lines.

The surface reconstruction on these grains is shown in Fig. 9(a). It has indeed a twofold, rhombohedral symmetry with a distance of 6.3 Å between nearest-neighbor corrugation maxima. The angle between the two sides of the unit cell (indicated by black dots) was measured to be $\sim 75°$. The characteristic linear chains along the short diagonal of the unit cell might consist of adsorbed excess Si. The orientation with respect to the Si substrate was determined by investigation of phase boundaries between the 2×2 reconstruction of the cubic phase and β-$FeSi_2$ grains in the temperature range of coexistence. Within the accuracy of STM angle measurements which is limited by piezo nonorthogonality and drift we find that the long diagonal of the surface unit cell points along Si$\langle \bar{2}11 \rangle$ and the short one along Si$\langle 01\bar{1} \rangle$. This allows a simple interpretation. In Fig. 9(b) we have drawn the Fe(001) plane composed of the atoms shown checkered in Fig. 7(b). By assuming that only every second atomic position is visible in STM topographs (due to buckling or electronic differences) one obtains a surface unit cell in good agreement with our observations. We do not want to imply that the surface must be Fe terminated, although this could be the case since the measured corrugation amplitudes of the reconstruction are relatively small, typically 0.3 Å. There could also be an additional Si layer on top which keeps the symmetry of the Fe plane. It has to be pointed out that the observed step height, close to half the length of the c axis, is in agreement with this model.

The (001) orientation could be of some practical relevance if one was able to use such layers as a template for thicker high-quality β-$FeSi_2$ films. Corresponding studies are currently under way. As a preliminary result Fig. 8(b) displays a 53-Å film grown by RT coevaporation of 22-Å stoichiometric $FeSi_2$ onto a (001)-oriented template. Afterwards it was annealed at 550 °C. The grooves indicate the grain size. The grain edges are faceted in two orthogonal directions from which one can determine the relative grain orientation. This shows that, in principle, the growth of thicker films is possible. The most intriguing problem which we are facing at the moment is how to further increase the domain size which will certainly be a prerequisite for good electro-optical properties.

3. β-$FeSi_2$ (100) ‖Si (111)

On films grown under the conditions described in the preceding section we sometimes observed another epitaxial orientation. It can occur simultaneously with the (001) grains. The grains can be as large in extent, in some cases even exceeding the 4-μm range of our scanner. The surface morphology is also similar. The two orientations can easily be distinguished by the surface step height which was measured to be 5–5.5 Å in this case. On the atomic scale we resolved a fourfold-symmetric reconstruction which is shown in Fig. 10(a): each square of atomic protrusions has a side length of 5.5 Å. The corrugation amplitude is only ~ 0.3 Å. The orientation with respect to the Si substrate was determined in the same way as described above. One diagonal of the quadratic unit cell was found to be parallel to the Si$\langle 1\bar{1}0 \rangle$ direction. From this we can determine the epitaxial orientation: The only atomic β-$FeSi_2$ planes compatible with a fourfold-symmetric surface reconstruction are the two inequivalent Fe(100) planes shown checkered in Fig. 7(a). They can well account for the observed 5.5-Å nearest-neighbor distance and the observed surface step height ($\sim a/2$). This results in the following relationship: β-$FeSi_2(100)$‖Si(111) with either β-$FeSi_2$[001] or [010]‖Si$\langle 1\bar{1}0 \rangle$. The mismatch for these epitaxial orientations is also relatively small: 2.0% (1.4%) along Si$\langle 1\bar{1}0 \rangle$ and −2.4% (−1.9%) along Si$\langle \bar{2}11 \rangle$. In TEM plan-view diffraction both orientations (with a clear predominance of the first one) have indeed been observed. In Fig. 10(b) an example for the first one is given. In some cases the fourfold surface reconstruction was found to be rotated by $\sim 15°$, such that one square side ran parallel to the $\langle 01\bar{1} \rangle$ direction of the cubic 2×2. This implies that the β-$FeSi_2$ [011] direction must be along Si$\langle 01\bar{1} \rangle$. This orientation has also been confirmed by TEM, which demonstrates that, by a careful analysis of the symmetry of the surface reconstruction, its orientation with respect to the substrate and the surface step height, epitaxial orientations can be determined rather reliably. For this third (100) orientation one could imagine a relatively simple interface structure: in the β-$FeSi_2$ unit cell the four Fe atoms shown dashed in Fig. 7(a) have

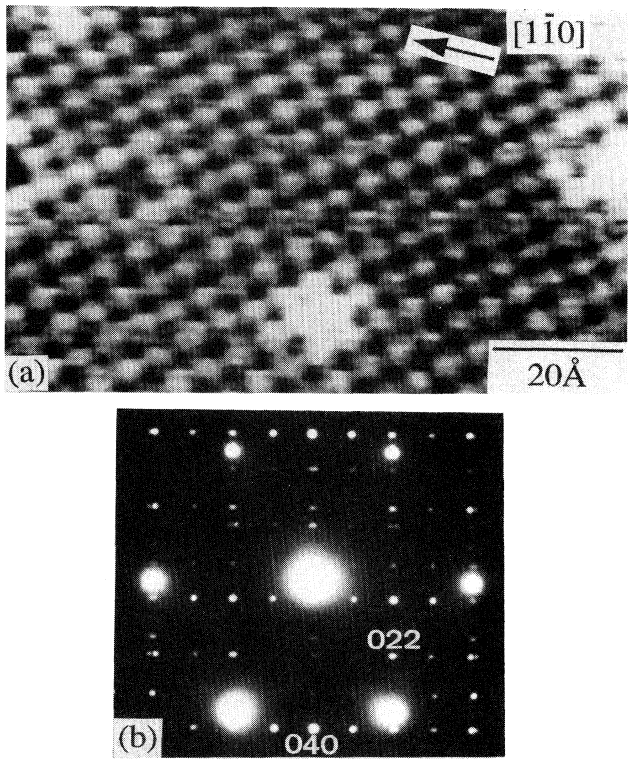

FIG. 10. (a) Filled-state CCT ($V_t=-0.5$ V, $I_t=1$ nA) of the fourfold surface reconstruction on (100)-oriented β-$FeSi_2$ ($d=23$ Å, $T_a=630$ °C), (b) corresponding selected-area plan-view TEM diffraction pattern taken along Si[111]. The β-$FeSi_2$ (004) spot coincides with the Si$\{02\bar{2}\}$ one.

essentially the same geometry as the atoms in the Si(111) planes. Locally, this could result in a favorable bonding configuration at the interface which would be possible for at least one cell within the common unit mesh $[3(b^2+c^2)^{1/2}\times(b^2+c^2)^{1/2}=33.1\ \text{Å}\times 11.0\ \text{Å}]$. For the first two orientations one must expect a relatively complicated interface due to the large common unit mesh ($5b\times c$ and $5c\times b$, respectively). To gain a more profound insight corresponding cross-sectional TEM investigations are planned to be performed in the future.

D. Discussion

In this section we first try to give an explanation for the surface corrugation described in Sec. III B.

The phenomenon could in principle be related to the relaxation of the elastic strain in the pseudomorphic phase. By XRD we have determined the geometrical mismatch η of as-grown $Fe_{1-x}Si$ as a function of the stoichiometry. For the monosilicide ($x=0$) it amounts to $\sim 2\%$. With decreasing Fe content it changes sign, resulting in a mismatch of $\sim -0.5\%$ for the disilicide ($x=0.5$).

It can be excluded that the contrast in STM topographs originates from misfit dislocations similar to that observed on $CoSi_2$/Si(111) and (100) (Ref. 19). In plan-view TEM the density of dislocations was found to be much lower than one would estimate from the corrugation wavelength. In this respect it has to be mentioned that sometimes the observed crests and valleys end somewhere on the surface without an apparent disruption in the atomic surface structure. A dislocation cannot end in the film bulk. It would either have to emerge at its surface or penetrate into the substrate and form a closed loop.

In Stranski-Krastanow systems such as Ge on Si(100), a strain-driven surface instability has recently been reported:[21] The substrate (100) planes become curved in order to allow for the relaxation of the surface in a coherent Ge island. Such a mechanism cannot directly be applied to our system since the pseudomorphic $FeSi_2$ films are two dimensional and continuous, i.e., a curvature of the (111) planes would lead to both expanded and compressed regions. However, in our specific case, the corrugation would necessarily have to be accompanied by lateral deviations from the average stoichiometry as determined by the deposition, i.e., Fe enrichment in the expanded regions. The silicide could then have its stoichiometry-dependent lattice constant everywhere at the surface with the film remaining coherent. The relevant driving force would be determined by the misfit of the pseudomorphic cubic phase,[22] which amounts to only -0.5% at RT. This value will be further reduced at the higher annealing temperatures since the thermal expansion of all disilicides exceeds that of Si by a factor of 2–4. It appears thus rather unlikely that the observed corrugation can be explained in terms of such a strain-driven surface instability.

We therefore propose a different explanation based on the structural similarity between the β-$FeSi_2$ and the CaF_2 crystal structure. It has been pointed out by Dusausoy *et al.*[3] that the orthorhombic phase can be understood as a Jahn-Teller-like distortion of the fluorite structure. The bonding configuration in both structures is quite similar: each metal atom has eight nearest Si neighbors which are situated on the edges of a cube with the metal atom in the center. In the orthorhombic structure these cubes are slightly distorted [see Fig. 7(a)]. The epitaxial orientation which would be expected if the phase transition took place between the cubic fluorite and the orthorhombic phase by a simple distortion of the unit cells without an overall rotation is the one described in Sec. III C 1. The β-$FeSi_2$(101) planes correspond to the fluorite (111) planes and have a distorted hexagonal symmetry. This is illustrated in Fig. 7(b), where the CaF_2 unit cells corresponding to the β-$FeSi_2$ one are indicated by dashed lines. The horizontal is thought to represent the Si(111) interface plane. The bulk lattice constants for β-$FeSi_2$ and the theoretically calculated one for the CaF_2 structure[8] have been used. Angles are also drawn to scale. The hypothetical transformation between the two phases could be mediated by a soft phonon mode of the cubic phase.

Within this framework we propose the following scenario for the phase transition: By annealing, the system is obviously driven towards β-$FeSi_2$. If thin films of the pseudomorphic phase are indeed stable at RT the transition can be due to a temperature dependence of the bulk free energy difference between the orthorhombic and the cubic structure. At some temperature the elastic energy gained by the pseudomorphic phase becomes insufficient to compensate for the bulk free energy loss. In the other possible case where the cubic structure is only metastable at RT the thermal energy might enable the system to overcome an activation barrier. Such a barrier will certainly exist in both cases since the relatively high misfit of β-$FeSi_2$ would require the nucleation of a dense array of misfit dislocations. This would not be true if the system just underwent a local Jahn-Teller-like distortion towards β-$FeSi_2$. If the lateral size of the distorted regions was smaller than the distance between two misfit dislocations in relaxed β-$FeSi_2$, then no dislocations would have to be introduced, i.e., the transition could proceed without a nucleation barrier. This state of small volumes with a β-$FeSi_2$-like structure within a cubic matrix would precede the actual phase transition. This model might account for the deteriorating Kikuchi bands and the observed surface corrugation. It would also explain why the crystal deterioration in thicker layers occurs at lower temperatures already since there the actual transition occurs earlier as well.[7] The driving force towards the stable bulk phase certainly increases with film thickness but also with annealing temperature. Therefore the distorted regions will tend to grow with increasing temperature. At some point they become so large that misfit dislocations will have to be introduced, which might be the reason for the observed change in defect structure of the pseudomorphic phase close to the transformation [see Fig. 5(b)].

If our notion is essentially correct one would have to expect an intermediate phase with the CaF_2 structure, designated γ-$FeSi_2$ (Ref. 7), since upon starting from the

low-temperature CsCl-derived phase the metal atoms would first have to undergo ordering into every second metal (111) plane.[13] At relatively high annealing temperatures close to the transition we have indeed found TEM cross sections with the fluorite symmetry. In Fig. 11 an example is shown for a 21-Å film annealed at 550 °C: In contrast to the low-temperature phase with the CsCl symmetry the reflexes with odd (*hkl*) are also present. The CaF_2 phase was not homogeneous, as cross sections with the CsCl symmetry were also found on the same sample. It has to be pointed out that the fluorite phase alone cannot account for the observed surface corrugation since it should be equally well lattice matched to Si as the CsCl-derived phase. Assuming the contrast to be of purely topographic origin, a 1-Å corrugation amplitude on a 20-Å film would require a difference in the perpendicular lattice constant of $\sim 5\%$. In this respect it might be worth recalling that at high annealing temperatures the 2×2 appears homogeneous both in filled- and empty-state CCT's. This also indicates that, at least at the surface, the metal sublattice becomes ordered. It should be pointed out that films thinner than ~ 10 Å appear to be thermally stable against a phase transition to β-$FeSi_2$. Since they can be annealed at rather high temperatures we suppose that they consist of homogeneous γ-$FeSi_2$.

Our model is nevertheless still speculative and further TEM investigations are required to directly image the distorted regions. Until now this has been hindered by the relatively small wavelength of the observed corrugation.

The phase transition from pseudomorphic $FeSi_2$ has also been studied in films grown by SPE (Ref. 5) and reactive deposition epitaxy (RDE).[23] It does not follow exactly the same path with respect to the thickness dependence and the nucleation of β-$FeSi_2$. We believe that this is mainly due to the drastically different kinetics. Apart from factors like substrate quality, growth and annealing rates, etc. the crucial variable governing phase transitions in epitaxial Fe silicides appears to be the stoichiometry of the initial phase. In SPE and RDE the stoichiometry is difficult to adjust because of the diffusion involved in the formation of the silicide, whereas the MBE method has the advantage that one can start from a pseudomorphic phase of well-defined composition. In addition, the island morphology of SPE- and RDE-grown films will also lead to different kinetics in the nucleation of the orthorhombic phase.

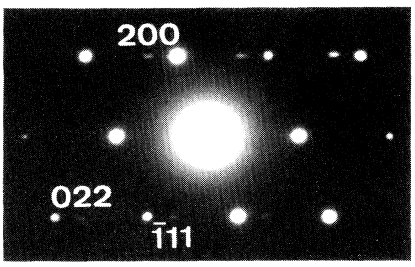

FIG. 11. Cross-sectional TEM diffraction pattern taken along the $[0\bar{1}1]$ direction with the CaF_2 symmetry. It was obtained on a 21-Å $FeSi_2$ film annealed at 550 °C. Only silicide spots are indexed (according to a cubic cell with the Si lattice parameter).

As a final point we want to comment on the critical influence of the initial film stoichiometry on the path of the phase transition. Experimentally, this is firmly established: If we do not rotate the sample during growth we can prepare films in which the Fe:Si ratio varies by $\sim 10\%$ across the wafer. In this way we can eliminate the influence of other parameters such as the details of the annealing procedure, substrate quality, etc. A corresponding experiment with a film of 32-Å thickness (in the center of the wafer) annealed at 500 °C confirmed the findings reported above: In the Fe-rich regions the transformation had already occurred; (100) and (001) β-$FeSi_2$ grains were observed. On the stoichiometric and Si-rich parts the morphology was similar to the one shown in Fig. 6(a). Theoretically, we do not yet understand the role which the additional Fe plays in determining the epitaxial orientation. Of course, the three orientations cannot differ much in their total energies (which contains contributions from the surface and interface and the energy required for the introduction of misfit dislocations). An important hint might be the observed lowering of the transformation temperature in slightly Fe-rich films. This might suggest that the driving force, i.e., the difference in the Gibbs free energy between the pseudomorphic and the stable bulk phase, is larger. This could be due to a decrease in the entropy of the cubic phase, since the additional Fe certainly decreases the number of possible configurations on the metal sublattice. The lower transition temperature could influence the epitaxial orientation via the thermal mismatch or purely kinetic factors. Alternatively, the Fe-rich stoichiometry might also directly affect the β-$FeSi_2$ nucleation, e.g., via a different atomic interface structure of the pseudomorphic phase, which could kinetically favor the nucleation of (100)- and (001)-oriented grains.

From a practical point of view it is important to find out if it is possible to further increase the grain size in the (001)-oriented β-$FeSi_2$ films. Quasi-single-crystalline layers can only be expected if one artificially removes the threefold symmetry of the Si substrate. The simplest way to achieve this is to use intentionally misoriented substrates.[24] Currently, we are performing experiments with different misorientation angles and directions hoping that in this way we can favor one of the three possible grain orientations. Probably, this would significantly improve the electro-optical properties of the β-$FeSi_2$ films, since grain boundaries usually act as effective recombination centers.

IV. CONCLUSIONS

To conclude, we have used the scanning tunneling microscope to study the temperature-induced phase transition from pseudomorphic $FeSi_2$ to β-$FeSi_2$ on Si(111). We determined the crystal structure of the as-grown pseudomorphic phase to be a CsCl-derived defect phase. In STM spectroscopy we found direct evidence for the atomic disorder on the metal sublattice. The fluorite

symmetry was only locally observed after prolonged annealing at temperatures near the transition to β-$FeSi_2$. Upon annealing a decrease in the crystalline order of the cubic phase occurred. It can be explained by a local structural distortion towards the orthorhombic phase which precedes the actual phase transition. The phenomenon could also be relevant in other systems where the pseudomorphic and the stable bulk phase are structurally similar. However, in cases of different bonding configurations it should not occur. This is in agreement with our results on the transition between pseudomorphic FeSi and ϵ-FeSi where the low-temperature phase remains well ordered up to the transition.[12] By using slightly Fe-rich deposition rates β-$FeSi_2$ films could be synthesized with a (001) and (100) orientation which do not occur in SPE-grown films. We have described in some detail the surface reconstructions observed on the different β-$FeSi_2$ grains and related them to the symmetry of the unreconstructed lattice planes. Due to their relatively high structural perfection with grains of several μm in size these orientations could mean some progress towards optical applications of epitaxial β-$FeSi_2$ films.

ACKNOWLEDGMENTS

It is a pleasure to thank P. Steiner and H. J. Gübeli for their excellent technical assistance. We also thank K. A. Mäder, S. Zehnder, and S. Goncalves-Conto for valuable contributions. Financial support from the Swiss National Science Foundation (NFP 24) is gratefully acknowledged.

[1]N. Cherief, C. D'Anterroches, R. C. Cinti, T. A. Nguyen Tan, and J. Derrien, Appl. Phys. Lett. **55**, 1671 (1989).

[2]N. Cherief, R. Cinti, M. de Crescenzi, J. Derrien, T. A. Nguyen Tan, and J. Y. Veuillen, Appl. Surf. Sci. **41/42**, 241 (1989).

[3]P. Y. Dusausoy, J. Protas, R. Wandji, and B. Roques, Acta. Crystallogr. Sec. B **27**, 1209 (1971).

[4]G. A. Prinz, Phys. Rev. Lett. **54**, 1051 (1985).

[5]J. Chevrier, V. Le Thanh, S. Nitsche, and J. Derrien, Appl. Surf. Sci. **56-58**, 438 (1992).

[6]M. G. Grimaldi, P. Baeri, C. Spinella, and S. Lagomarsino, Appl. Phys. Lett. **60**, 1132 (1992).

[7]N. Onda, J. Henz, E. Müller, H. von Känel, C. Schwarz, and R. E. Pixley, Helv. Phys. Acta **64**, 197 (1991); N. Onda, J. Henz, E. Müller, K. A. Mäder, and H. von Känel, Appl. Surf. Sci. **56-58**, 421 (1992).

[8]N. E. Christensen, Phys. Rev. B **42**, 7148 (1990).

[9]J. de la Figuera, A. L. Vàzquez de Parga, J. Alvarez, J. Ibánez, C. Ocal, and R. Miranda, Surf. Sci. **264**, 45 (1992).

[10]H. von Känel, R. Stalder, H. Sirringhaus, N. Onda, and J. Henz, Appl. Surf. Sci. **53**, 196 (1991); for a recent review, see, e.g., H. von Känel, Mater. Sci. Rep. **8**, 193 (1992).

[11]R. Stalder, H. J. Gübeli, H. von Känel, and P. Wachter, Rev. Sci. Instrum. **63**, 1676 (1992).

[12]H. von Känel, K. A. Mäder, E. Müller, N. Onda, and H. Sirringhaus, Phys. Rev. B **45**, 13 807 (1992).

[13]H. von Känel, N. Onda, H. Sirringhaus, E. Müller-Gubler, S. Goncalves-Conto, and C. Schwarz, Appl. Surf. Sci. (to be published).

[14]A. L. Vazquez de Parga, J. de la Figuera, C. Ocal, and R. Miranda, Europhys. Lett. **18**, 595 (1992).

[15]J. P. Pelz and R. H. Koch, Phys. Rev. B **42**, 3761 (1990); J. J. Boland, Surf. Sci. **244**, 1 (1991).

[16]R. J. Hamers, R. M. Tromp, and J. E. Demuth, Phys. Rev. Lett. **56**, 1972 (1986).

[17]J. A. Stroscio and R. M. Feenstra, in *Scanning Tunneling Microscopy*, edited by J. A. Stroscio and W. J. Kaiser (Academic, New York, 1991).

[18]R. M. Feenstra, J. A. Stroscio, and A. P. Fein, Surf. Sci. **181**, 295 (1987).

[19]R. Stalder, H. Sirringhaus, N. Onda, and H. von Känel, Appl. Phys. Lett. **59**, 1960 (1991).

[20]D. Gerthsen, K. Radermacher, Ch. Dieker, and S. Mantl, J. Appl. Phys. **71**, 3788 (1992).

[21]D. J. Eaglesham and M. Cerullo, Phys. Rev. Lett. **64**, 1943 (1990).

[22]R. Bruinsma and A. Zangwill, J. Phys. (Paris) **47**, 2055 (1986).

[23]J. Alvarez, A. L. Vázquez de Parga, J. J. Hinarejos, J. de la Figuera, E. G. Michel, C. Ocal, and R. Miranda, Appl. Surf. Sci. (to be published).

[24]J. Derrien, J. Chevrier, V. le Thanh, and J. E. Mahan, Appl. Surf. Sci. **56-58**, 382 (1992).

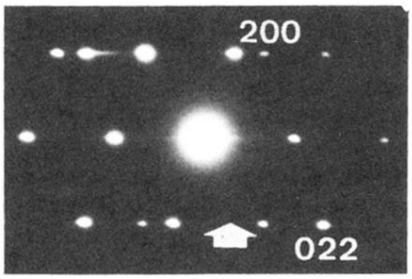

FIG. 1. Cross-sectional TEM diffraction pattern of an as-grown $FeSi_2$ film with the CsCl symmetry taken along the $[01\bar{1}]$ direction. Only the silicide spots are indexed according to a cubic cell with the Si lattice parameter.

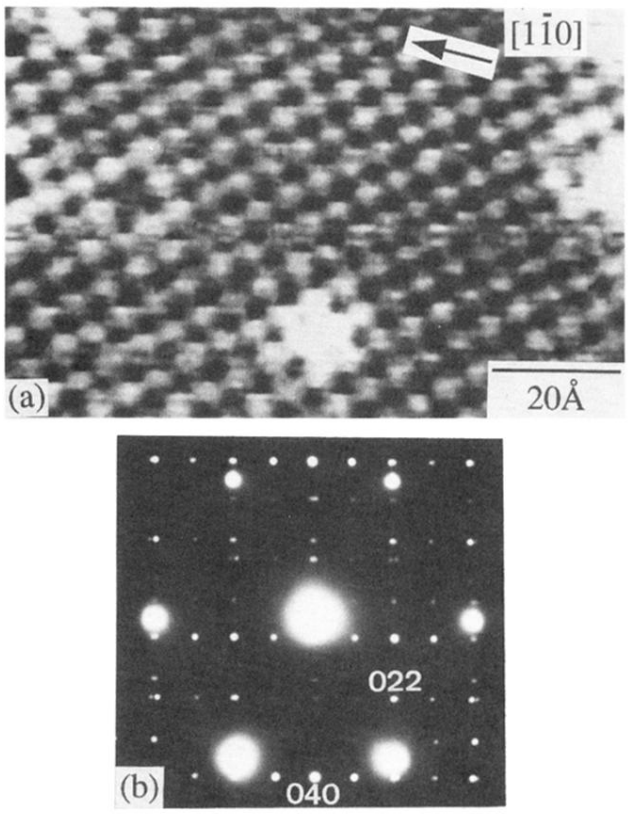

FIG. 10. (a) Filled-state CCT ($V_t = -0.5$ V, $I_t = 1$ nA) of the fourfold surface reconstruction on (100)-oriented β-$FeSi_2$ ($d = 23$ Å, $T_a = 630$°C), (b) corresponding selected-area plan-view TEM diffraction pattern taken along Si[111]. The β-$FeSi_2$ (004) spot coincides with the Si$\{02\bar{2}\}$ one.

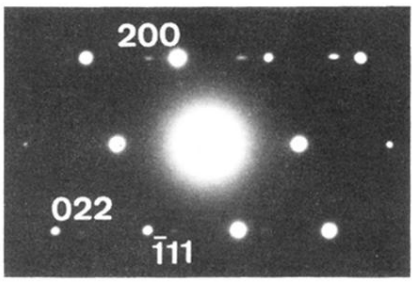

FIG. 11. Cross-sectional TEM diffraction pattern taken along the $[0\bar{1}1]$ direction with the CaF_2 symmetry. It was obtained on a 21-Å $FeSi_2$ film annealed at 550 °C. Only silicide spots are indexed (according to a cubic cell with the Si lattice parameter).

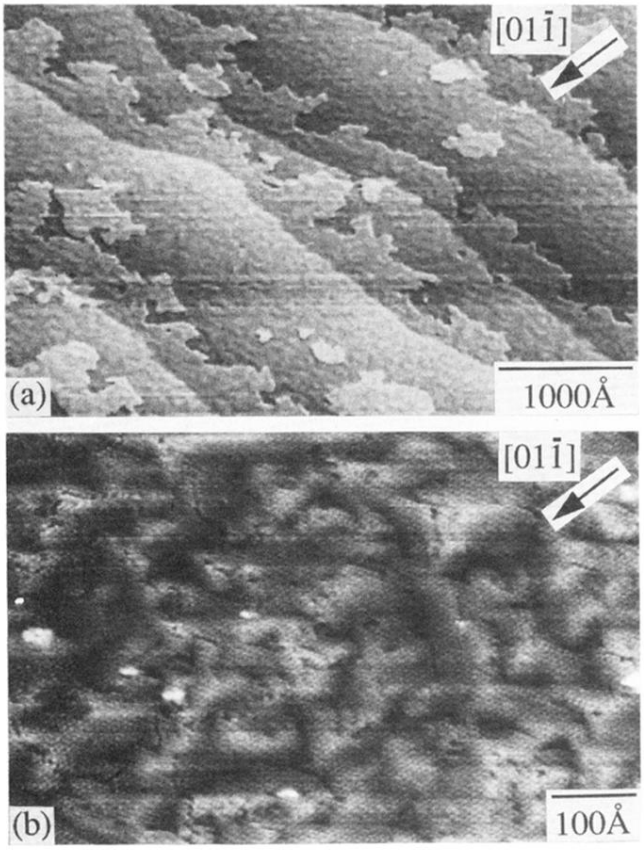

FIG. 2. STM topographs obtained on pseudomorphic $FeSi_2$ displaying (a) the mesoscopic surface morphology (sample bias voltage $V_t = 1$ V, tunneling current $I_t = 1$ nA, film thickness $d = 21$ Å, annealing temperature $T_a = 500\,^{\circ}\mathrm{C}$) and (b) the surface corrugation ($V_t = 1.5$ V, $I_t = 2$ nA, $d = 21$ Å, $T_a = 500\,^{\circ}\mathrm{C}$).

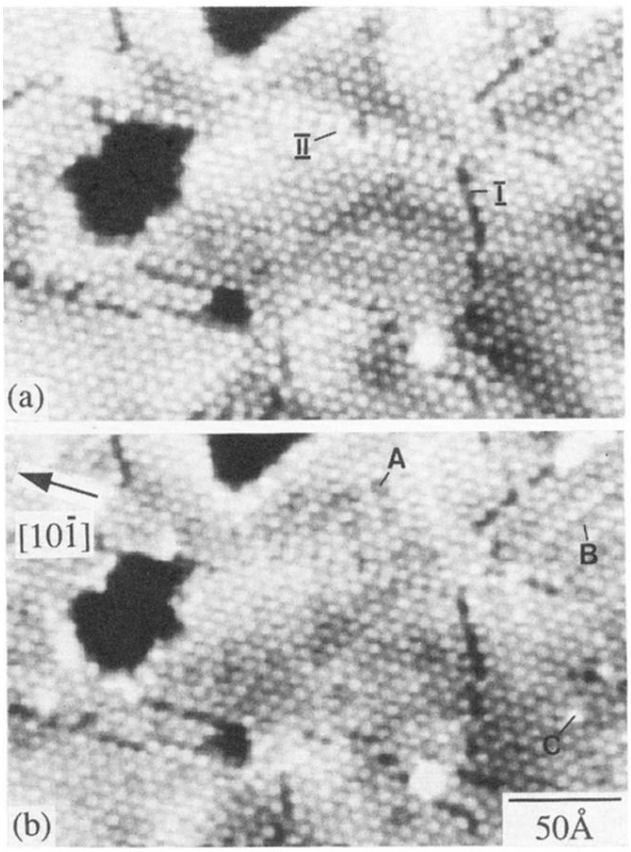

FIG. 3. Atomic resolution STM topographs of the 2×2 surface reconstruction ($d=16$ Å, $T_a=500$ °C): (a) empty-state image ($V_t=2$ V, $I_t=0.5$ nA), (b) filled-state image ($V_t=-2$ V, $I_t=0.5$ nA). I and II denote the two different types of 2×2 domain boundaries. Sites with significant voltage dependencies are labeled by letters.

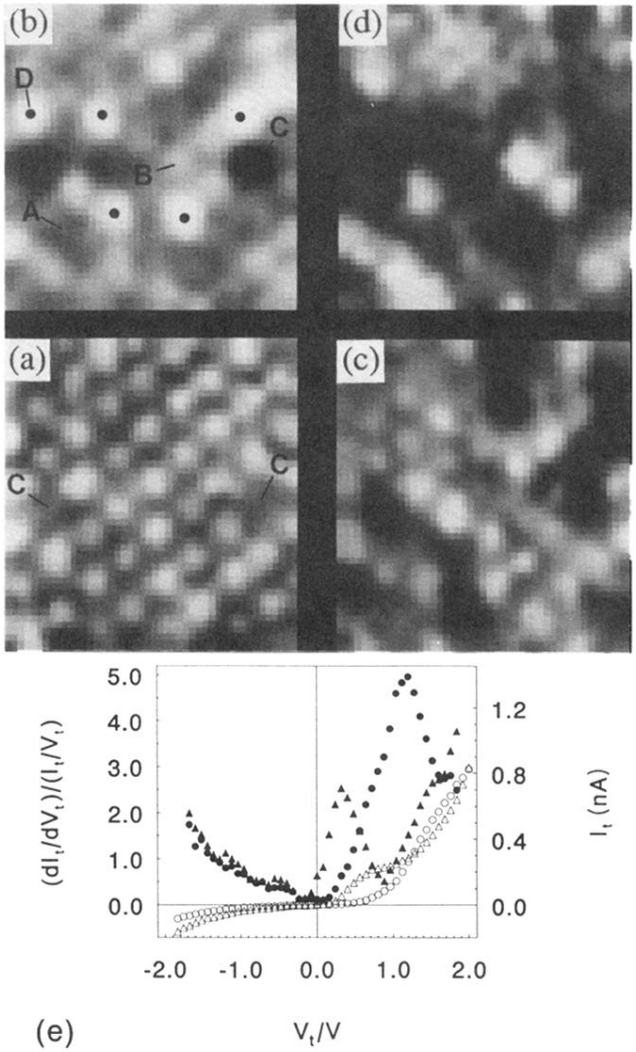

FIG. 4. Constant-current topographs (CCT) and current images (CI) of the 2×2 on ultrathin films ($d=7$ Å, $T_a=500$ °C): (a) empty-state CCT ($V_t=2$ V, $I_t=1$ nA), (b) filled-state CCT ($V_t=-2$ V, $I_t=1$ nA), (c) CI at $V_t=1.35$ V, (d) CI at $V_t=0.3$ V measured with a stabilization voltage and current of 2 V and 1 nA, respectively (in the CI, areas of high current appear bright), (e) current-voltage (open symbols) and normalized conductivity (filled symbols) curves belonging to the depressed (A, circles) and bright (B, triangles) sites of the filled-state CCT in (b).

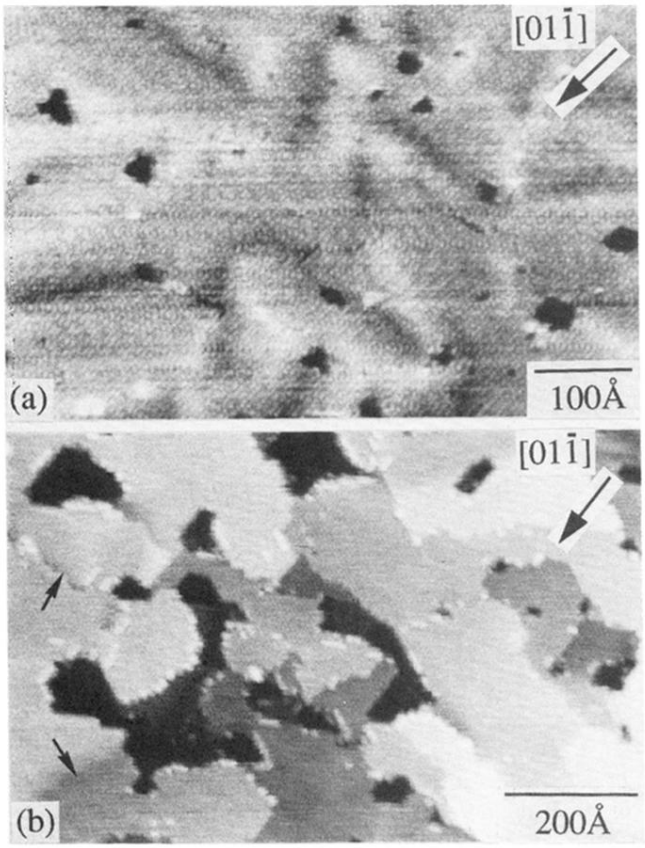

FIG. 5. STM topographs illustrating the evolution of the surface corrugation at higher annealing temperatures ($d = 17$ Å): (a) after 550 °C ($V_t = 1.6$ V, $I_t = 1$ nA), (b) after 600 °C ($V_t = 1.8$ V, $I_t = 0.5$ nA).

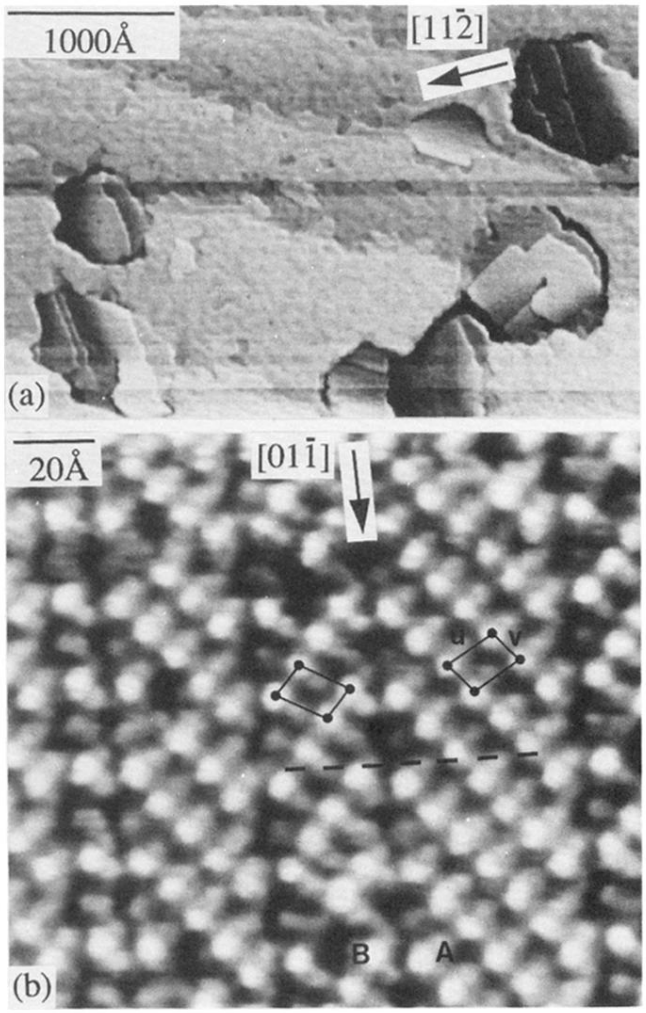

FIG. 6. STM topographs of (101)-oriented β-$FeSi_2$ grains: (a) nucleation of β-$FeSi_2$ grains within the cubic matrix ($d=31$ Å, $T_a=500$ °C, $V_t=1.5$ V, $I_t=1$ nA), (b) empty-state CCT of the surface reconstruction ($d=53$ Å, $T_a=630$ °C, $V_t=2$ V, $I_t=4$ nA) (in all STM images directions are indexed with respect to the Si substrate). The unit cells (solid lines) on domains A and B can be transformed into each other by a glide plane operation. The dashed line indicates the line of intersection of the mirror plane with the surface.

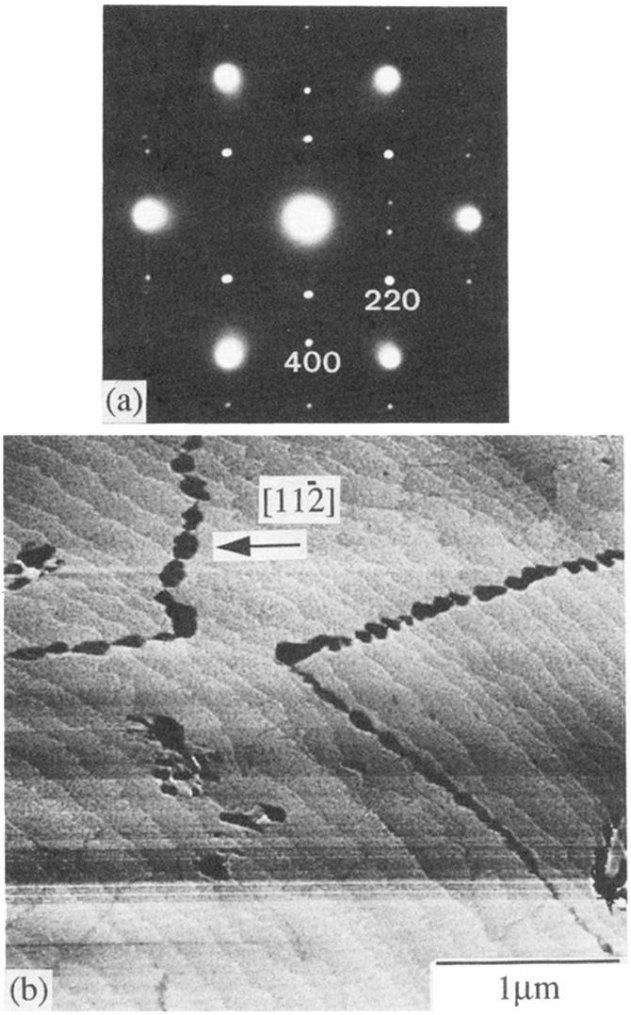

FIG. 8. (a) Selected-area plan-view TEM diffraction pattern of (001)-oriented β-$FeSi_2$ ($d=26$ Å, $T_a=480$ °C) taken along Si[111]. The bright spots with sixfold symmetry are the Si$\{02\bar{2}\}$ spots, (b) large area STM topograph ($V_t=2$ V, $I_t=1$ nA) obtained on a 53-Å-thick β-$FeSi_2$ film grown by using a (001)-oriented β-$FeSi_2$ film with 31-Å thickness as a template ($T_a=550$ °C).

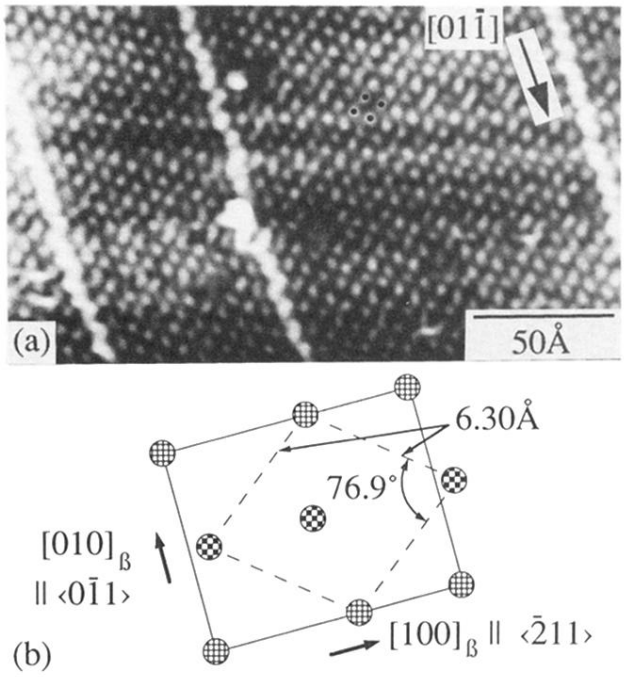

FIG. 9. (a) Empty-state CCT displaying the surface reconstruction on (001)-oriented β-$FeSi_2$ ($V_t = 0.2$ V, $I_t = 0.2$ nA, $d = 26$ Å, $T_a = 600$ °C). A surface unit cell is indicated by black dots, (b) schematic model for the reconstruction in (a) based on the Fe(001) planes shown checkered in Fig. 7(b). The unit cell observed in STM is indicated by dashed lines.